

Optimal foraging strategies can be learned and outperform Lévy walks

Gorka Muñoz-Gil,^{1,*} Andrea López-Incera,^{1,*} Lukas J. Fiderer,¹ and Hans J. Briegel¹

¹*Institute for Theoretical Physics, University of Innsbruck, Technikerstr. 21a, A-6020 Innsbruck, Austria*

Lévy walks and other theoretical models of optimal foraging have been successfully used to describe real-world scenarios, attracting attention in several fields such as economy, physics, ecology, and evolutionary biology. However, it remains unclear in most cases which strategies maximize foraging efficiency and whether such strategies can be learned by living organisms. To address these questions, we model foragers as reinforcement learning agents. We first prove theoretically that maximizing rewards in our reinforcement learning model is equivalent to optimizing foraging efficiency. We then show with numerical experiments that our agents learn foraging strategies which outperform the efficiency of known strategies such as Lévy walks.

Strategies to search for randomly distributed targets are of paramount importance in many fields. For instance, they are widely used in ecology to model the foraging activities of predators [1], hunters [2] and gatherers [3], as well as the movement of pedestrians in complex environments [4]; other interesting applications are the study of human information search in complex knowledge networks [5] or the improvement of optimization algorithms [6].

A widely used and investigated idealization of such search problems is the model of non-destructive foraging (cf. Fig. 1). The model consists of a two-dimensional environment with randomly, uniformly, and sparsely distributed immobile targets which can be detected by a walker within a *detection radius* r . The walker moves through the environment with constant speed in steps (straight segments) of random orientation and varying *step length* L . As soon as the walker detects a target, its current step is aborted, whereupon it immediately takes its next step from a position displaced in a random direction by a *cutoff length* $l_c > r$ from the detected target.

The goal of the walker is to maximize the search efficiency

$$\eta = \lim_{T \rightarrow \infty} \frac{n_T}{T} \quad (1)$$

where T is physical time and n_T is the average number (with respect to target positions) of detected targets in the time interval $[0, T]$. In several fields, η^{-1} is known as the mean first-passage time (MFPT) since it equals the average time a walker needs to detect the first target [7]. Indeed, MFPT-based approaches are widely used to study and compare different search strategies [8–11]. However, the hardness of computing the MFPT in realistic scenarios poses an obstacle to the theoretical understanding of optimal search strategies.

Non-destructive foraging corresponds to the biologically relevant case of foraging replenishable targets where larger cutoff lengths l_c correspond to longer replenishment times of targets [12]. In particular, the case of *destructive* foraging, where targets vanish after detection, can formally be recovered by taking the limit $l_c \rightarrow \infty$.

Motivated by observational data [13–15] and supported by heuristic arguments [15–17], a family of step-length distributions known as Lévy distributions [18, 19] $\Pr(L) \propto s^\mu L^{-\mu}$, where s is a length-scale parameter and $\mu \in [0, 2]$, received major attention, including the discovery of the optimal value of μ in certain limiting cases [7, 17], such as $l_c \rightarrow \infty$ and $l_c \rightarrow r$. While a number of numerical studies have shown that typically the optimal value of μ depends sensitively on the environmental parameters [7, 12, 17, 20, 21], it has recently been shown that other families of step-length distributions $\Pr(L)$ such as bi- and tri-exponential distributions outperform Lévy distributions [8, 22, 23]. In general, it is still an open problem what strategy is optimal for non-destructive foraging, both in terms of its step-length distribution family and its precise parameters.

Given the good agreement of theory and observational data of animals, another debate concerns the question of how animals come to possess knowledge of particular search strategies, which recently sparked interest from a neurological perspective [24, 25]. More generally, the origin of search strategies is usually classified as either *emergent* or *evolutionary* [26]. The former considers that an individual walker can learn *different* strategies via complex interactions with different environments, while the latter proposes that a *single* strategy has evolved via natural selection in order to optimize search in different environments [27]. In order to understand emerging and adaptive processes one has to go beyond the study of optimal search strategies based on heuristic ansätze; it calls for a framework that naturally incorporates learning.

In this paper we introduce such a framework, based on reinforcement learning (RL), and demonstrate the advantages it offers to understand the appearance of (optimal) search strategies as a result of learning.

Non-destructive foraging in the RL framework.— We base our framework on RL, a standard paradigm of machine learning [28] that considers an agent interacting with an environment (see Fig. 1). During each interaction cycle, called an *RL step*, the agent perceives *state* $s \in \mathcal{S}$ from the environment, and replies with an *action* $a \in \mathcal{A}$. We adopt the common assumption that the agent is Markovian, which means that the probability $\pi(a|s)$ that the agent chooses action a only depends

* These authors contributed equally to the work

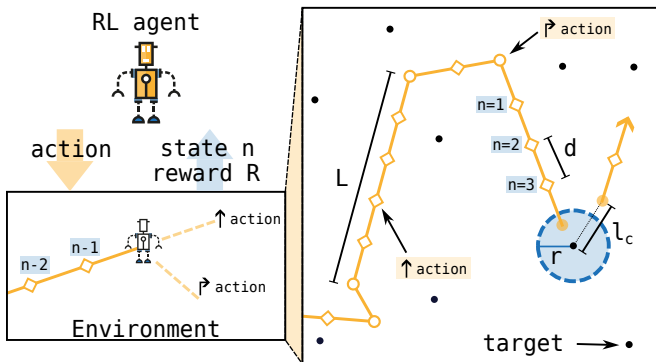


FIG. 1. The problem of non-destructive foraging is formulated within the framework of RL. An agent moves through an environment with randomly distributed targets and, at each step, chooses between two possible actions: continue in the same direction (\uparrow) or turn (\uparrow^r) in a random direction. The state perceived by the agent is a counter n , which is the number of small steps of length d which compose the current step of length L . Whenever the agent detects a target, it receives a reward R and resumes its walk at a distance l_c from the detected target with the counter reset.

on the current state s . $\pi(a|s)$ is called the *policy* of the RL agent. Further, we consider the environment to be partially observable, which means that the agent cannot perceive the full state $e \in \mathcal{E}$ of the environment, that is $s \neq e$.

The agent also receives a *reward* signal $R(e, a)$ depending on the current action a and the state of the environment e . The goal of the agent is then to optimize its policy such that the expected average reward

$$R_\pi(e) = \lim_{T \rightarrow \infty} \frac{\mathbb{E} \left[\sum_{t=0}^T R(e_t, a_t) \middle| \pi, e_0 = e \right]}{T} \quad (2)$$

is maximized, where $t \in \mathbb{N}_0$ labels the RL steps and \mathbb{E} denotes expectation with respect to all infinite trajectories of agent-environment interactions given that the agent employs policy π and that the environment is initially in state $e \in \mathcal{E}$. In practice, the optimization of Eq. (2) with respect to the policy π is governed by an RL algorithm which will be discussed further below.

In the following, we embed non-destructive foraging within the framework of RL. The idea is to model the walker as a Markovian agent. A naive approach would be to let the agent choose its step length L in each RL step. However, this would correspond to an infinite action space \mathcal{A} which often represents an obstacle to efficient learning. Instead, we opt for a more feasible implementation by discretizing the step length L in units of *small steps* d such that at each RL step the agent only has the following choice: either continue in the direction of its previous step or *turn* in a random direction. This approach is arguably closer to biological reality since the agent makes decisions at regular intervals rather than walking for a potentially very long time before making

the next decision. Moreover, in more complex scenarios, such an agent can better adapt to changes in the environment.

To this end, given the environmental parameters r , l_c , and d , which characterize the search problem, the state of the environment is defined by the positions of targets, together with the current position, walking direction, and a *step counter* $n \in \mathbb{N}$ of the agent. The counter is reset to $n = 1$ whenever the agent turns or detects a target and it increases by one whenever the agent continues without detecting a target. In each RL step, the counter is perceived by the agent, i.e., $s = n$. The two possible actions are *continue* and *turn*, symbolically denoted by \uparrow and \uparrow^r , which correspond to walking for a distance d either in the current or in a random direction, respectively. If the agent detects a target, its position is resampled at a distance l_c from the detected target, according to the non-destructive foraging model. Then, the agent walks a small step of length d in a random direction, and it perceives the counter state $n = 1$ and a reward $R = 1$. Otherwise, when no target is detected, $R = 0$ and the agent continues its walk unimpeded.

The probability that the agent makes a step of length L is thus given by

$$\Pr(L = Nd) = \pi(\uparrow^r | N) \prod_{n=1}^{N-1} \pi(\uparrow | n), \quad (3)$$

where we use the convention that the empty product, in case of $N = 1$, equals one. Since there are only two actions, we have $\pi(\uparrow^r | n) = 1 - \pi(\uparrow | n)$.

We proceed by showing that our RL agent maximizes its search efficiency η by maximizing the expected average reward in Eq. (2). First we note that the average number of targets detected during the first T RL steps, given that policy π is employed and that the environment is initially in state e , can be written as

$$n_T = \mathbb{E} \left[\sum_{t=0}^T R(e_t, a_t) \middle| \pi, e_0 = e \right], \quad (4)$$

since $R = 1$ when a target is detected and $R = 0$ otherwise. By inserting Eq. (4) into the definition of the detection efficiency, Eq. (1), we immediately see that $\eta = R_\pi(e)$ and therefore, η is maximal when $R_\pi(e)$ is. This proves an important feature of our RL formulation of foraging: reinforcement learning converges to optimal search strategies.

Since our RL formulation moves the focus from step-length distributions $\Pr(L)$ to policies π , we proceed to show which policy will reproduce a given step-length distribution. Policy and step-length distribution are related via Eq. (3). Inserting $\pi(\uparrow | N) = 1 - \pi(\uparrow^r | N)$ into Eq. (3) yields a recurrent equation for $\pi(\uparrow^r | n)$, the solution of which we find to be

$$\pi(\uparrow^r | N) = \frac{\Pr(L = Nd)}{1 - \sum_{n=1}^{N-1} \Pr(L = nd)} \quad (5)$$

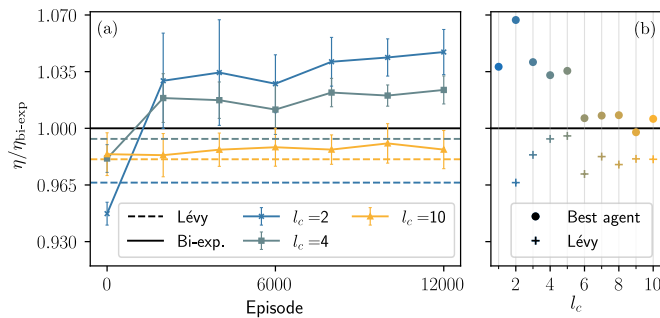


FIG. 2. Learning curves and the advantage of learned policies over benchmarks. (a) The search efficiency (averaged over 10 agents, displayed with one standard deviation) is shown over the course of learning (measured in training episodes). Different colors correspond to environments with different cutoff length l_c . Efficiencies are normalized by the respective best benchmark efficiency, which turns out to be bi-exponential distributions in all cases. Dashed lines show the efficiency of the best Lévy walk for each case. (b) Comparison between the best agent’s search efficiency at the end of learning and that of the best benchmarks, for each environment. The efficiency of the best Lévy walk for $l_c = 1$ is $\eta_{\text{Lévy}}/\eta_{\text{bi-exp.}} = 0.88$. For each agent and benchmark model, the efficiency is averaged over $2 \cdot 10^8$ RL steps. In panel b), the standard error of the mean for the benchmark models and the best agents is depicted but too small to be visible.

for any N such that the denominator is non-vanishing, i.e., $\sum_{n=1}^{N-1} \Pr(L = nd) \neq 1$, or equivalently, $\sum_{n=N}^{\infty} \Pr(L = nd) \neq 0$. If $\sum_{n=N}^{\infty} \Pr(L = nd) = 0$, no step can continue beyond length $(N-1)d$, which implies $\pi(r^* | n) = 1$ for an $n < N$. In this case, the agent would always turn before perceiving states with $n \geq N$. It is straightforward to verify that Eq. (5) leads to $\Pr(Nd)$ -distributed step lengths by inserting Eq. (5) into Eq. (3). From Eq. (5) it can also be seen that the agent must employ a probabilistic policy to reproduce arbitrary step-length distributions; deterministic policies with $\pi(s|a) \in \{0, 1\}$ can only generate walks with constant step lengths.

Numerical case study.— In the framework of RL, learning consists of updating the policy in order to maximize the obtained rewards (Eq. (2)) in response to agent-environment interactions. From a plethora of RL algorithms, we choose projective simulation (PS) [29, 30] (for details, see Appendix B and [31]). We expect that similar results can be found with other RL algorithms such as policy gradient [28].

As benchmarks for the trained RL agents, we use the widely investigated Lévy walks [7, 15, 17, 18] as well as the strongest ansatz considered in the literature so far: a random walk with bi-modal exponential step length distribution [8, 22, 23] (see Appendix A for details). Their search efficiencies are computed numerically by simulating an agent with an equivalent, fixed policy, obtained via Eq. (5), which for short will be referred to as Lévy and bi-exponential policies, respectively.

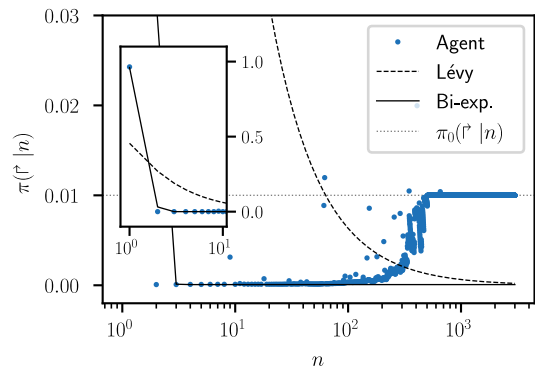


FIG. 3. Policy of an RL agent trained in an environment with cutoff length $l_c = 0.6$. The policies corresponding to the best bi-exponential (solid line, $d_1 = 0.15, \omega_1 = 0.96, d_2 = 13047.89$) and the best Lévy distributions (dashed line, $\beta = 0.64$) are shown for comparison. The normalized search efficiencies are $\eta_{\text{RL}}/\eta_{\text{bi-exp}} = 1.02$ and $\eta_{\text{Lévy}}/\eta_{\text{bi-exp}} = 0.85$. The grey dotted line marks the initialization policy $\pi_0(r^* | n) = 0.01 \forall n$.

It is important to note that an RL agent is not expected to learn any of the benchmark policies unless these are the only ones that maximize search efficiency (i.e. these strategies are indeed optimal). Nevertheless, we want to demonstrate, from a numerical perspective, that an RL agent based on PS has the capacity to learn any of these policies. To this end, we train agents to imitate the benchmark policies with various parameters and find a near-perfect convergence of their learned policies (for further details on imitation learning, see Appendix B 1). These results suggest that, if any of the known foraging strategies is optimal, we can expect a trained agent converging to it. With this result in mind, we return to the original problem of learning optimal foraging strategies by interacting with an environment with randomly distributed targets, see Fig. 1.

We model the infinite foraging environment by a two-dimensional squared box of size $W = 100$ with periodic boundary conditions, 100 randomly distributed targets (thus corresponding to a target density $\rho = 0.01$) with a detection radius $r = 0.5$, where the unit length is defined as the small-step size of the agent $d = 1$. In what follows, we consider that all lengths are measured in units of $d = 1$ and we adopt a dimensionless notation. In this work, the agents are always initialized with a policy $\pi_0(r^* | n) = 0.01 \forall n$. Further details on this and the respective parameters of the learning process are presented in Appendix B.

We simulate RL agents in various foraging environments with different cutoff length l_c . Fig. 2 shows the learning curves of the agents, i.e., the evolution of search efficiency over the course of learning (see Appendix B 2 for details). The performance averaged over 10 agents reaches or overcomes the best benchmark in most cases, showing the robustness of the proposed RL method. Importantly, in all but one of the tested environments,

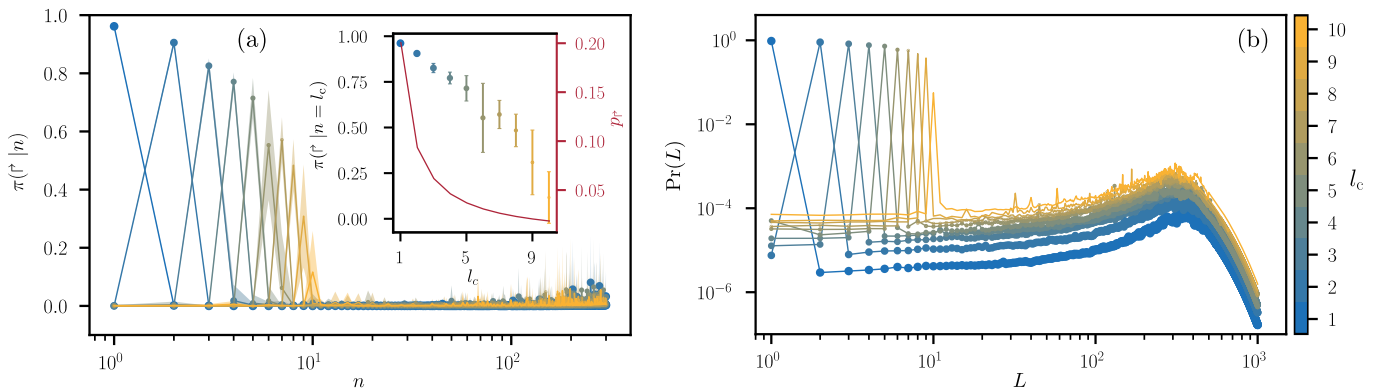


FIG. 4. Analysis of the learned policies for different cutoff lengths. (a) Learned policies $\pi(r|n)$ as a function of the counter n . Each point is the average over 10 agents and the shaded area represents one standard deviation. The inset shows, on the left axis, the turning probability at $n = l_c$ averaged over 10 agents, error bars represent one standard deviation. On the right axis, the probability p_r of hitting the target when turning at $n = l_c$ is shown (see Appendix C). (b) Step-length distributions corresponding to the policies presented in a). Each point is the median over 10 agents.

the best of the 10 trained agents achieves higher efficiency than the respectively best benchmark model (see Fig. 2b), suggesting that there exist optimal strategies beyond the benchmark model families.

In order to better understand the learned policies and the origin of such an advantage, we start by comparing the learned policy with the benchmarks at the example of $l_c = 0.6$, see Fig. 3. For $n \lesssim 10^2$, training significantly changes the initial policy, and the learned policy shows greater similarity to the bi-exponential than to the Lévy policy. For $n \gg 10^2$, the learned policy still equals its initial value of 0.01. This is due to practical limitations of the training and can in particular be attributed to a limited training time, as detailed in Appendix B3. However, note that the policy for large n only affects the agent’s behavior at sufficiently long steps that happen very rarely, and thus the resulting effect on the agent’s walk is rather small.

Fig. 4a shows the learned policies for environments with $l_c \in [1, 10]$, revealing an interesting property of the learned policies: the probability of turning at $n = l_c$ is significantly increased for all environments considered, and the smaller l_c the more pronounced this effect is (see inset of Fig. 4a). This can be understood by an approximation: in the regime of low target density and small l_c , after the detection of a target, to a good approximation the immediate environment of the agent only contains the previously detected target. Then, apart from the possibility of returning to the target by walking straight for l_c , there is a significant probability p_r that the agent will first miss the target if it walks straight for l_c but then detects the target in the next step by turning at $n = l_c$, see inset of Fig. 4a. This explains the added benefit of turning at $n = l_c$ (for details, see Appendix C).

Using Eq. (3), we translate the learned policies from Fig. 4a into the their corresponding step-length distributions (Fig. 4b). The learned distributions show a pronounced peak at $L = l_c$, which can be interpreted as the

agents learning to forage with a length scale related to the cutoff length. Then, for $10^1 \lesssim L \lesssim 10^2$, we find a region where the probability remains stable, i.e., with a smaller probability the agents also make longer steps, associated with a second and larger length scale. For $L > 10^2$, $\text{Pr}(L)$ increases before it decreases exponentially, which is due to the finite training times (see Appendix B3). This prevents us from fully characterizing the second length scale (and any other that might appear for larger L), which is commonly related to the average spacing between targets [23].

Indeed “two-scale” foraging strategies, such as the bi-exponential benchmark, have been widely studied in the literature [22, 26, 27] and their approximate emergence from our learning model is interesting. It should be noted, however, that this emergence is only approximate: first, we found the learned policies to perform even slightly better than the bi-exponential benchmark in most cases. Second, neither the learned step-length distributions are fully characterized by two scales, nor is the problem of non-destructive foraging, since the detection radius r represents a third length scale [23]. Therefore there are good reasons to hope for learning advantages over benchmark model families, as found in this work.

Discussion. — We introduced a framework based on reinforcement learning (RL) for non-destructive foraging in environments with sparsely distributed immobile targets. The framework is based on analytic results which involve an exact correspondence between the policy $\pi(a|n)$ and the step-length distribution $\text{Pr}(L)$ of the agent, and a proof that learning converges to optimal foraging strategies. This not only makes the proposed RL framework a viable alternative to traditional approaches, but also introduces remarkable benefits.

Firstly, learning is not restricted to a specific ansatz, as e.g. step-length distributions such as Lévy walks or bi-exponential ansätze, which have been extensively studied in the literature. Even in cases where the latter are op-

timal, RL could be leveraged to find the suitable parameters of the respective model family. Most importantly, RL together with Eq. (3) paves the way for the discovery of novel, more efficient step-length distributions.

Secondly, the RL framework sidesteps the problem of what knowledge about the environment (e.g., characteristic length scales) should be considered available to the agent; while it is often assumed that foragers do not possess any knowledge about the environment, it is also well-known that informed agents usually outperform their agnostic counterparts [23, 27]. With RL, it is not necessary to artificially endow the agent with knowledge about the environment. Instead, the agent implicitly *learns* such knowledge by interacting with the environment. Interestingly, recent work has also shown that RL agents create implicit maps of their environments even when they are not directly programmed to do so [32]. As shown in our numerical case study, RL agents are able to adapt to different length scales of the environment. Therefore, the assumption that foragers do not possess any knowledge about the environment is unrealistic for adaptive, learning foragers.

The proposed framework could also be leveraged to understand how search strategies are learned by foragers in biological scenarios. This is related to the debate on the emergent versus evolutionary hypotheses (see Introduction). Both evolutionary priors and learning could be modelled within our framework via policy initialization and policy updating, respectively. For example, we showed numerically (Fig. 2) that an agent initialized with a preference for walking straight efficiently learns to per-

form better than Lévy searches.

Moreover, we expect RL to be beneficial especially when dealing with more complex environments, where exploiting the numerous properties of the environment can lead to better foraging strategies. Some examples include complex topographies [21], non-uniform distributions of targets [27], the presence of gradient forces or obstacles, or even self-interacting foragers [33]. Moreover, RL can be used to study multi-agent scenarios [30, 34] and their connection with known collective phenomena such as flocking [35, 36].

ACKNOWLEDGMENTS

We acknowledge Michele Caraglio and Harpreet Kaur for insightful discussions. This work was supported by the Austrian Science Fund (FWF) through the SFB BeyondC F7102, and the European Research Council (ERC, QuantAI, Project No. 10105529). A.L and H.J.B also acknowledge support by the Volkswagen Foundation (Az:97721). G.M-G also acknowledges funding from the European Research Council under the Marie Skłodowska-Curie grant agreement No. 101063794. Views and opinions expressed are however those of the author(s) only and do not necessarily reflect those of the European Union or the European Research Council. Neither the European Union nor the granting authority can be held responsible for them.

-
- [1] David W Sims, Emily J Southall, Nicolas E Humphries, Graeme C Hays, Corey JA Bradshaw, Jonathan W Pitchford, Alex James, Mohammed Z Ahmed, Andrew S Briereley, Mark A Hindell, et al. Scaling laws of marine predator search behaviour. *Nature*, 451(7182):1098–1102, 2008.
 - [2] David A Raichlen, Brian M Wood, Adam D Gordon, Audax ZP Mabulla, Frank W Marlowe, and Herman Pontzer. Evidence of Lévy walk foraging patterns in human hunter–gatherers. *Proceedings of the National Academy of Sciences*, 111(2):728–733, 2014.
 - [3] Clifford T Brown, Larry S Liebovitch, and Rachel Glendon. Lévy flights in dove ju/’hoansi foraging patterns. *Human Ecology*, 35(1):129–138, 2007.
 - [4] Hisashi Murakami, Claudio Feliciani, and Katsuhiko Nishinari. Lévy walk process in self-organization of pedestrian crowds. *Journal of the Royal Society Interface*, 16(153):20180939, 2019.
 - [5] David M Lydon-Staley, Dale Zhou, Ann Sizemore Blevins, Perry Zurn, and Danielle S Bassett. Hunters, busybodies and the knowledge network building associated with deprivation curiosity. *Nature human behaviour*, 5(3):327–336, 2021.
 - [6] Xin-She Yang and Suash Deb. Cuckoo search via Lévy flights. In *2009 World congress on nature & biologically inspired computing (NaBIC)*, pages 210–214. Ieee, 2009.
 - [7] Nicolas Levernier, Johannes Textor, Olivier Bénichou, and Raphaël Voituriez. Inverse square Lévy walks are not optimal search strategies for $d \geq 2$. *Physical review letters*, 124(8):080601, 2020.
 - [8] Vladimir V Palyulin, Aleksei V Chechkin, and Ralf Metzler. Lévy flights do not always optimize random blind search for sparse targets. *Proceedings of the National Academy of Sciences*, 111(8):2931–2936, 2014.
 - [9] Jean-François Rupprecht, Olivier Bénichou, and Raphaël Voituriez. Optimal search strategies of run-and-tumble walks. *Physical Review E*, 94(1):012117, 2016.
 - [10] A Chechkin and IM3845437 Sokolov. Random search with resetting: a unified renewal approach. *Physical review letters*, 121(5):050601, 2018.
 - [11] Vladimir V Palyulin, Vladimir N Mantsevich, Rainer Klages, Ralf Metzler, and Aleksei V Chechkin. Comparison of pure and combined search strategies for single and multiple targets. *The European Physical Journal B*, 90(9):1–16, 2017.
 - [12] EP Raposo, Sergey V Buldyrev, MGE Da Luz, MC Santos, H Eugene Stanley, and Gandhi Mohan Viswanathan. Dynamical robustness of Lévy search strategies. *Physical review letters*, 91(24):240601, 2003.
 - [13] Blaine J Cole. Fractal time in animal behaviour: the movement activity of drosophila. *Animal Behaviour*, 50(5):1317–1324, 1995.
 - [14] FL Schuster and M Levandowsky. Chemosensory re-

- sponses of *acanthamoeba castellanii*: visual analysis of random movement and responses to chemical signals. *Journal of Eukaryotic Microbiology*, 43(2):150–158, 1996.
- [15] Gandhimohan M Viswanathan, Vsevolod Afanasyev, Sergey V Buldyrev, Eugene J Murphy, Peter A Prince, and H Eugene Stanley. Lévy flight search patterns of wandering albatrosses. *Nature*, 381(6581):413–415, 1996.
- [16] M Levandowsky, J Klafter, and BS White. Swimming behavior and chemosensory responses in the protistan microzooplankton as a function of the hydrodynamic regime. *Bulletin of Marine Science*, 43(3):758–763, 1988.
- [17] Gandimohan M Viswanathan, Sergey V Buldyrev, Shlomo Havlin, MGE Da Luz, EP Raposo, and H Eugene Stanley. Optimizing the success of random searches. *nature*, 401(6756):911–914, 1999.
- [18] Micheal F Shlesinger, George M Zaslavsky, and Uriel Frisch. Lévy flights and related topics in physics. 1995.
- [19] Vasily Zaburdaev, Sergey Denisov, and Joseph Klafter. Lévy walks. *Reviews of Modern Physics*, 87(2):483, 2015.
- [20] MC Santos, EP Raposo, GM Viswanathan, and MGE Da Luz. Optimal random searches of revisitable targets: crossover from superdiffusive to ballistic random walks. *EPL (Europhysics Letters)*, 67(5):734, 2004.
- [21] Giorgio Volpe and Giovanni Volpe. The topography of the environment alters the optimal search strategy for active particles. *Proceedings of the National Academy of Sciences*, 114(43):11350–11355, 2017.
- [22] Simon Benhamou and Julien Collet. Ultimate failure of the Lévy foraging hypothesis: Two-scale searching strategies outperform scale-free ones even when prey are scarce and cryptic. *Journal of theoretical biology*, 387:221–227, 2015.
- [23] J Ferreira, EP Raposo, HA Araújo, MGE da Luz, GM Viswanathan, Frederic Bartumeus, and Daniel Campos. Landscape-scaled strategies can outperform Lévy random searches. *Physical Review E*, 103(2):022105, 2021.
- [24] Sabrina A Jones, Jacob H Barfield, V Kindler Norman, and Woodrow L Shew. Scale-free behavioral dynamics directly linked with scale-free cortical dynamics. *bioRxiv*, pages 2021–05, 2022.
- [25] David W Sims, Nicolas E Humphries, Nan Hu, Violeta Medan, and Jimena Berni. Optimal searching behaviour generated intrinsically by the central pattern generator for locomotion. *Elife*, 8:e50316, 2019.
- [26] Andy Reynolds. Liberating Lévy walk research from the shackles of optimal foraging. *Physics of life reviews*, 14:59–83, 2015.
- [27] Marina E Wosniack, Marcos C Santos, Ernesto P Raposo, Gandhi M Viswanathan, and Marcos GE Da Luz. The evolutionary origins of Lévy walk foraging. *PLoS computational biology*, 13(10):e1005774, 2017.
- [28] Richard S Sutton and Andrew G Barto. *Reinforcement learning: An introduction*. MIT press, 2018.
- [29] Hans J Briegel and Gemma De las Cuevas. Projective simulation for artificial intelligence. *Scientific reports*, 2(1):1–16, 2012.
- [30] A. López-Incera, K. Ried, T. Müller, and H. J. Briegel. Development of swarm behavior in artificial learning agents that adapt to different foraging environments. *PLoS ONE*, 15(12):e0243628, 2020.
- [31] Gorka Muñoz Gil, Andrea López-Incera, Lukas J. Fiderer, and Hans J. Briegel. RL-OptS: Reinforcement learning of optimal search strategies. https://github.com/gorkamunoz/rl_opts, 2023.
- [32] Erik Wijmans, Manolis Savva, Irfan Essa, Stefan Lee, Ari S. Morcos, and Dhruv Batra. Emergence of maps in the memories of blind navigation agents. In *The Eleventh International Conference on Learning Representations*, 2023.
- [33] A Barbier-Chebbah, O Bénichou, and R Voituriez. Self-interacting random walks: Aging, exploration, and first-passage times. *Physical Review X*, 12(1):011052, 2022.
- [34] Andrea López-Incera, Morgane Nouvian, Katja Ried, Thomas Müller, and Hans J Briegel. Honeybee communication during collective defence is shaped by predation. *BMC biology*, 19(1):1–16, 2021.
- [35] MC Santos, EP Raposo, GM Viswanathan, and MGE da Luz. Can collective searches profit from Lévy walk strategies? *Journal of Physics A: Mathematical and Theoretical*, 42(43):434017, 2009.
- [36] Adam Gosztolai, Jose A Carrillo, and Mauricio Barahona. Collective search with finite perception: transient dynamics and search efficiency. *Frontiers in Physics*, page 153, 2019.
- [37] Aaron Clauset, Cosma Rohilla Shalizi, and Mark EJ Newman. Power-law distributions in empirical data. *SIAM review*, 51(4):661–703, 2009.
- [38] Richard Liaw, Eric Liang, Robert Nishihara, Philipp Moritz, Joseph E Gonzalez, and Ion Stoica. Tune: A research platform for distributed model selection and training. *arXiv preprint arXiv:1807.05118*, 2018.
- [39] Julian Mautner, Adi Makmal, Daniel Manzano, Markus Tiersch, and Hans J Briegel. Projective simulation for classical learning agents: a comprehensive investigation. *New Gener. Comput.*, 33(1):69–114, 2015.
- [40] Adi Makmal, Alexey A Melnikov, Vedran Dunjko, and Hans J Briegel. Meta-learning within projective simulation. *IEEE Access*, 4:2110–2122, 2016.
- [41] Alexey A Melnikov, Adi Makmal, Vedran Dunjko, and Hans J Briegel. Projective simulation with generalization. *Sci. Rep.*, 7:14430, 2017.
- [42] W. L. Boyajian, J. Clausen, L. M. Trenkwalder, V. Dunjko, and H. J. Briegel. On the convergence of projective-simulation-based reinforcement learning in Markov decision processes. *Quantum Machine Intelligence*, 2:13, 2020.

Appendix A: Benchmark models

This appendix defines the model families used as benchmarks. These include i) the family of Lévy distributions [37],

$$\Pr(L) = \zeta_{(1+\beta,1)}^{-1} L^{-1-\beta}, \quad (\text{A1})$$

where $\zeta_{(1+\beta,1)} = \sum_{\ell=0}^{\infty} (\ell+1)^{-1-\beta}$ is the Riemann zeta function, and ii) the family of discrete bi-exponential distributions [37]

$$\Pr(L) = \sum_{i=1,2} \omega_i (1 - e^{-1/d_i}) e^{-(L-1)/d_i}, \quad (\text{A2})$$

where d_i are length scales and the mode weights satisfy $\sum_{i=1,2} \omega_i = 1$. Note that in each case we consider that the minimum step length is $L = 1$.

The search efficiency (Eq. (1)) of benchmark models and trained policies are computed the same way. To this end, the step-length distribution of a benchmark model is translated into an equivalent, fixed policy using Eq. (5), and then the average search efficiency is obtained from 10^4 walks, each consisting of $T = 20000$ small steps of length $d = 1$.

With a method to calculate the average search efficiency at hand, the model parameters are optimized in order to maximize the average search efficiency for both model families and for each environment (differing in cutoff length). We use Bayesian optimization for the family of bi-exponential distributions and grid searches for the Lévy distributions, via the Tune Python package [38], to obtain the model parameters that optimize the performance of each of the benchmark models for the environment under consideration. Fig. 5 shows the performance of each of the benchmark models for different values of the model parameters. We take the distributions that achieve the highest search efficiency for benchmarking. Examples of such optimizations are presented in the Tutorials section of the accompanying repository [31].

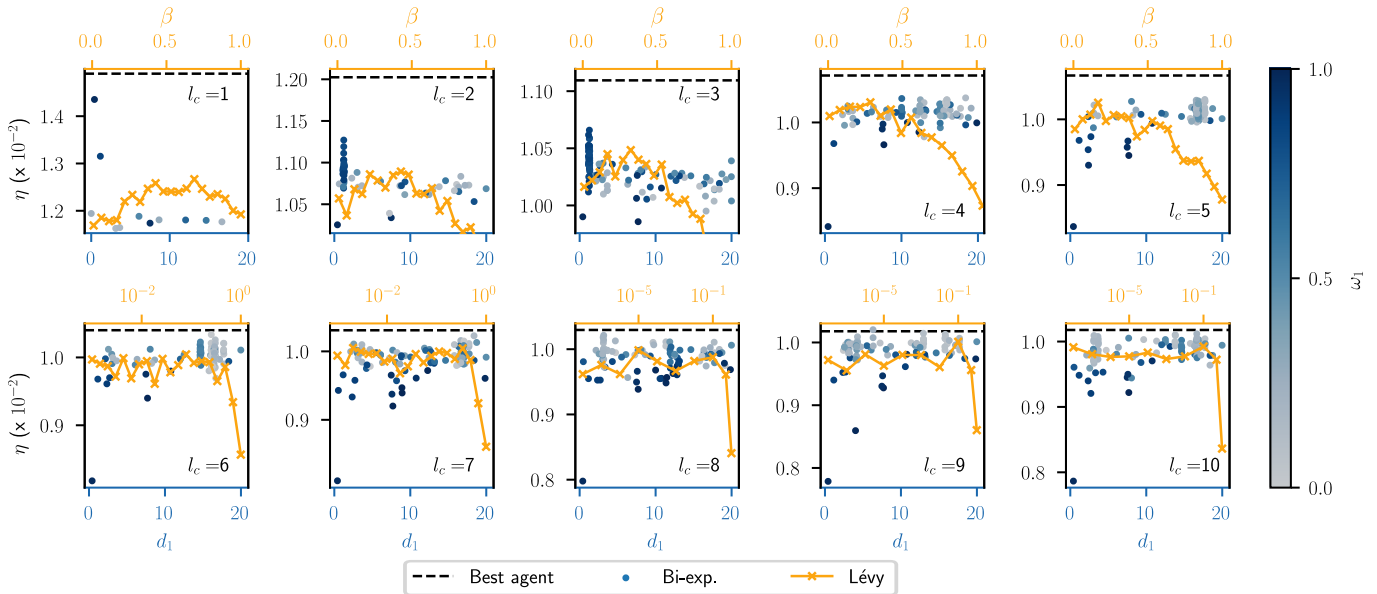


FIG. 5. Average search efficiency (η) achieved by agents with step-length distributions given by Eq. (A1) (Lévy) and Eq. (A2) (Bi-exponential), for different values of their model parameters, in environments with different cutoff length l_c . We use this search to find the Lévy and bi-exponential distributions that achieve the highest efficiency to benchmark the RL agent's performance. In all panels, each point shows the average over 10^4 walks. In panels with $l_c = 1, 3$, $d_2 = 10^5$. In panels with $l_c = 2, 4, 5, 6, \dots, 10$, $d_2 = 10^2$. Dashed lines indicate the efficiency of the best RL agent in each case.

Appendix B: Projective simulation

We use projective simulation (PS) [29, 39–41] to model the RL agent and its learning process. PS agents process the environmental information, that is, decide and learn by means of an episodic memory (ECM), which is mathematically described by a graph.

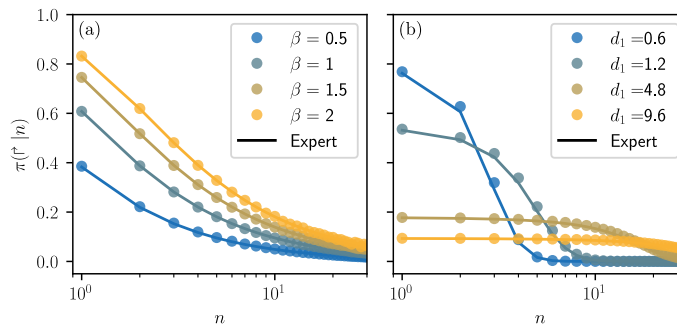


FIG. 6. Comparison of benchmark policies (solid lines) with the policies (colored dots) of a PS agent using imitation learning. Panel a) shows Lévy distributions with varying exponent β and panel b) shows bi-exponential distributions with varying d_1 , $w_1 = 0.94$ and $d_2 = 5000$ (see Appendix A for details).

In the simplest case, the nodes of this graph are distributed in two layers, one of which represents the states and the other the actions. Each state is connected to all possible actions by directed, weighted edges. The decision making of a PS agent is stochastic: the probability of performing action $a \in \mathcal{A}$ having perceived a state $s \in \mathcal{S}$ is

$$\pi(a|s) = \frac{h(s, a)}{\sum_{a' \in \mathcal{A}} h(s, a')}, \quad (\text{B1})$$

where $h(s, a)$, called h -value, is the weight of the edge that connects s with a . The agent learns by updating the h -values—and thus, its policy $\pi(a|s)$ —at the end of each RL step. During one interaction with the environment, i.e., one RL step, the agent (i) perceives a state s , (ii) decides on an action a by sampling from its current policy $\pi(a|s)$ and performs the action, (iii) receives a reward R from the environment, and (iv) updates its memory accordingly. The latter is implemented by updating the matrix \mathcal{H} that contains the h -values:

$$\mathcal{H} \leftarrow \mathcal{H} - \gamma(\mathcal{H} - \mathcal{H}_0) + \mathcal{G}R, \quad (\text{B2})$$

where γ is a damping factor that controls how quickly the agent forgets, \mathcal{H}_0 is the initial \mathcal{H} matrix and \mathcal{G} is the so-called glow matrix, which allows the agent to learn from delayed rewards, i.e. rewards that are only received several interactions with the environment later. The glow mechanism tracks which edges in the ECM were traversed prior to getting a reward. To do so, whenever there is a transition from state s to action a , its corresponding edge “glows” with a certain intensity given by the glow value $g(s, a)$, which is stored in the \mathcal{G} matrix. The glow has an initial value of $g(s, a) = 0$ and increases by 1 every time the edge is traversed (for details on the definition and update of the \mathcal{G} matrix, see [39, 42]). At the end of each RL step, \mathcal{G} is damped as

$$\mathcal{G} \leftarrow (1 - \eta_g)\mathcal{G}, \quad (\text{B3})$$

where η_g is the damping factor. Both η_g and γ are considered hyperparameters of the model and are adjusted to obtain the best learning performance.

1. Imitation learning of benchmarks

In this section, we study whether a PS agent is actually able to learn known foraging strategies within the proposed framework. To do so, we translate the original foraging problem into an imitation problem. Imitation learning is commonly used to simplify reinforcement learning problems with sparse rewards. Instead of learning in the original, complex scenario, the RL agent is trained to imitate an *expert* already equipped with the optimal policy. The expert is then considered to perform only succeeding trajectories, i.e. sets of actions that lead to rewarded states. In this way, the reward sparsity of the original problem can be avoided and learning the optimal policy is greatly simplified. Nonetheless, the RL agent is still required to correctly update its policy, hence imitation learning is a useful experiment to understand if the proposed framework is adequate for an agent that needs to learn optimal foraging strategies.

In what follows, we consider environments for which we assume that certain distributions $\text{Pr}(L)$ are optimal. This means that the expert’s policy is calculated inserting $\text{Pr}(L)$ in Eq. (5). In the imitation scheme, one RL step proceeds as follows:

1. a step of length L is sampled from $\text{Pr}(L)$;

2. the counter n of the RL agent is set to N such that $Nd = L$;
3. the agent RL performs the turning action, hence having effectively done a step of exactly length L ;
4. a reward $R = 1$ is given to the agent after the action (\uparrow) in state (N);
5. the agent updates its policy via Eq. (B2) based on this reward;

In Fig. 6a-b we show the convergence of the policy of an RL agent trained to imitate an expert equipped with policies calculated from Lévy and bi-exponential distributions with multiple parameters. As shown, the agent’s policy correctly converges to the expert’s. This ensures that the proposed framework, together with the PS update rule, can adequately accommodate the most typical foraging strategies, if these were to be optimal in the given environment.

2. Details about the training and the model parameters of the agent

The RL learning process of the PS agent consists of $N_{\text{ep}} \simeq 10^4$ episodes, each of which contains T RL steps. The agent’s memory has a two-layer structure of states and actions, as described in the previous section. Its learning mechanism is governed by Eq. (B2). There are T states, one for each possible value that the counter n can in principle take before the episode is over; and 2 actions, continue in the same direction or turn. At the beginning of each episode, the \mathcal{G} matrix of the agent is reset and both the agent’s position and the positions of the targets are randomly sampled. The agent keeps updating its policy until N_{ep} episodes are completed. In order to accurately assess search efficiency at different stages of training (Fig. 2), we perform a post-training evaluation: we take the policy in a given episode, freeze it, and have the agent employ this policy to perform 10^4 walks consisting of 20000 small steps of length $d = 1$ in environments with different target distributions. We train 10 independent agents in each scenario (given by different cutoff lengths) and consider that the best agent is the one that achieves the highest average search efficiency in the post-training evaluation using the policy after the last episode.

The learning parameters γ and η_g were adjusted in order to achieve the best performance in each case. The values of all parameters for each scenario are given in Table I. Examples of trainings are presented in the accompanying repository [31].

	Figs. 6 and 7c	Figs. 2 to 4	Fig. 7a-b
$\pi_0(\uparrow n)$	0.5	0.99	0.5
N_{ep}	1000	12000	69000
T	10000	20000	3000
η_g	10^{-7}	0.1	0.1
γ	0	10^{-5}	10^{-6}

TABLE I. Training parameters used to obtain the data presented in the respective figures.

3. Policy initialization and finite training times

In this section, we motivate our choice of policy initialization. In the literature, the policy of a PS agent is typically initialized such that $\pi_0(\uparrow | n) = \pi_0(\uparrow^r | n) = 0.5$ holds for all n . While $\pi_0(\uparrow^r | n) = 0.01$ is used in the main text, in this appendix, we first consider the $\pi_0(\uparrow^r | n) = 0.5$ policy initialization instead. That is, the agent initially chooses randomly and uniformly between the two possible actions \uparrow and \uparrow^r . In PS, this is enforced by setting all h -values in the initial \mathcal{H}_0 matrix to $h(s, a) = 1 \forall s, a$. As we see in Fig. 7a, the agent progressively learns to decrease $\pi(\uparrow^r | n)$, which in turn leads to longer steps, and to the agent reaching larger values of n as the learning progresses. Nonetheless, reaching large n is still exponentially costly. Moreover, to properly train the policy at a given n , the agent needs to first reach such value and then sample enough rewards. In Fig. 7b we show the frequency with which n is observed in different episodes. As expected, due to the update of the policy, the probability of reaching larger n increases as the training progresses. However, this training requires large computation times and still the agent does not sample steps longer than $L = 40$.

As can be seen in Fig. 7a, even after 69000 episodes (yellow line), the policy exhibits a decay back to initialization values for large n . The policy $\pi(\uparrow^r | n)$ at a given n depends not only on the received rewards at such n , but also on the rewards that will be attained for $n' > n$ due to the glow (Eq. (B3)). Thus, not reaching $n' > n$ also hampers the policy update of $\pi(\uparrow^r | n)$.

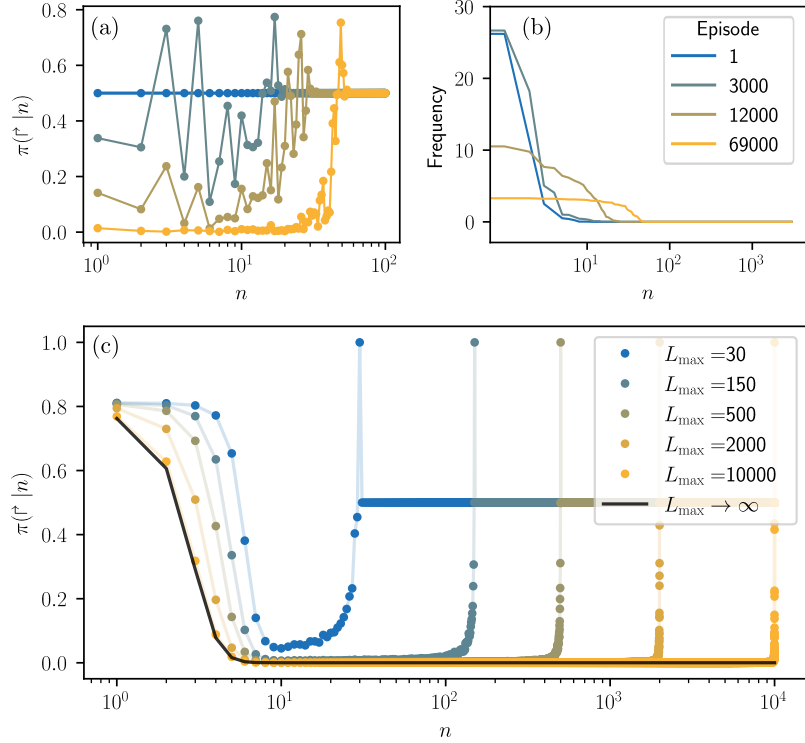


FIG. 7. a) Evolution of the policy throughout the learning process for one agent initialized with $\pi_0(\uparrow | n) = 0.5$ for all n . b) Frequency (in percentage of RL steps) with which the agent perceives each of the states n at a given episode (the color code for each episode is the same in panels a and b). Parameters are $l_c = 10$, $d = 1$, $r = 0.5$, and $\rho = 0.01$. c) Learned policies for imitation learning (for details, see Appendix B 1). The policy that corresponds to the distribution without cutoff ($L_{\max} \rightarrow \infty$) is shown for reference. Parameters are $d_1 = 0.6$, $d_2 = 5000$, and $\omega_1 = 0.94$.

Although imitation learning bypasses this problem (see Appendix B 1), it can still be used to further understand the effect of the problem on the trained policies. In Fig. 7c, we consider an agent that learns to imitate a bi-exponential distribution that has a cutoff at L_{\max} , such that $\Pr(L \geq L_{\max}) = 0$. As we see, the policy decays at $n \sim L_{\max}$. Moreover, the smaller L_{\max} , the more the policy at small n deviates from that of the bi-exponential distribution without cutoff ($L_{\max} \rightarrow \infty$).

To improve the exploration of longer steps, instead of increasing the training time, we change the initialization of the policy so that the agent takes longer steps more frequently already at the beginning of the training. In particular, throughout the numerical experiments presented in the main text, we consider that $\pi_0(\uparrow | n) = 0.01$ for all n , which is implemented by setting the h -values in the initial \mathcal{H}_0 matrix to $h(s, \uparrow) = 0.99$, and $h(s, \uparrow) = 0.01 \forall s$.

Appendix C: Efficiency advantage of turning at $nd \simeq l_c$

In this appendix, we outline a geometric argument which supports the observation that learned policies show an increase in the probability of turning after $nd \simeq l_c$ steps.

Let l_c be much smaller than $\sqrt{\rho^{-1}}$ (i.e. much smaller than the mean spacing between targets), and consider the following situation: an agent has detected a target and has just been displaced by l_c . Then, within a radius of l_c of the agent, there is typically no other target than the one previously detected. Let us therefore assume that the only target nearby is the one previously detected. Then, the environment for the next $nd \simeq l_c$ steps of the agent only contains the previously detected target, see Fig. 8. We write $nd \simeq l_c$ rather than $nd = l_c$ because l_c does not have to be an integer multiple of d . n is chosen such that it is possible to return to the target and to detect it by walking straight for precisely n steps, $n = \lceil \frac{l_c - r}{d} \rceil$.

We consider two probabilities: (i) the probability p_{\uparrow} that the agent returns directly to the target by walking straight for $nd \simeq l_c$, and (ii) the probability p_r that the agent returns to the target by first walking straight for nd (without detecting the target) and then walking for one step of length d at a random angle (it turns). It is a matter of simple trigonometric considerations to compute these probabilities. p_r is plotted in the inset of Fig. 4a. We find numerically

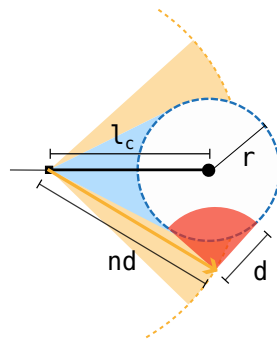


FIG. 8. Schematic illustration of the benefit of turning after $nd \simeq l_c$ steps in a simplified scenario with only a single target, the center of which is represented with a black dot and which has a detection radius r . After the detection of the target, the agent is displaced by a distance l_c from the target (black line). Then, we assume that it continues to walk straight for $nd \simeq l_c$ at a random angle (orange line). In this case, the blue area marks the angle range within which the agent returns to the target when walking straight. The yellow area indicates the angle range at which the target is missed but is still within reach (after one step) if the agent turns by a suitable angle (red area).

that p_r is even larger than p_{\uparrow} for the values of l_c plotted in the inset of Fig. 4a.